Chaos
An Interdisciplinary Journal of Nonlinear Science

Melnikov-type method for a class of planar hybrid piecewise-smooth systems with impulsive effect and noise excitation: Heteroclinic orbits

Cite as: Chaos **32**, 103127 (2022); https://doi.org/10.1063/5.0106073
Submitted: 27 June 2022 • Accepted: 19 September 2022 • Published Online: 31 October 2022

Zhouchao Wei, Yuxi Li, Irene Moroz, et al.

Melnikov-type method for a class of planar hybrid piecewise-smooth systems with impulsive effect and noise excitation: Heteroclinic orbits

Cite as: Chaos **32**, 103127 (2022); doi: 10.1063/5.0106073
Submitted: 27 June 2022 · Accepted: 19 September 2022 ·
Published Online: 31 October 2022

Zhouchao Wei,[1,2,a)] Yuxi Li,[1] Irene Moroz,[3] and Wei Zhang[4]

AFFILIATIONS

[1]School of Mathematics and Physics, China University of Geosciences, Wuhan 430074, China
[2]Zhejiang Institute, China University of Geosciences, Hangzhou, Zhejiang 311305, China
[3]Mathematical Institute, University of Oxford, Oxford OX2 6GG, United Kingdom
[4]College of Mechanical Engineering, Beijing University of Technology, Beijing 100124, China

Note: This article is part of the Focus Issue, Non-smooth Dynamics.
[a)]**Author to whom correspondence should be addressed:** weizhouchao@163.com

ABSTRACT

The classical Melnikov method for heteroclinic orbits is extended theoretically to a class of hybrid piecewise-smooth systems with impulsive effect and noise excitation. We assume that the unperturbed system is a piecewise Hamiltonian system with a pair of heteroclinic orbits. The heteroclinic orbit transversally jumps across the first switching manifold by an impulsive effect and crosses the second switching manifold continuously. In effect, the trajectory of the corresponding perturbed system crosses the second switching manifold by applying the reset map describing the impact rule instantaneously. The random Melnikov process of such systems is then derived by measuring the distance of perturbed stable and unstable manifolds, and the criteria for the onset of chaos with or without noise excitation is established. In this derivation process, we overcome the difficulty that the derivation method of the corresponding homoclinic case cannot be directly used due to the difference between the symmetry of the homoclinic orbit and the asymmetry of the heteroclinic orbit. Finally, we investigate the complicated dynamics of a particular piecewise-smooth system with and without noise excitation under the reset maps, impulsive effect, and non-autonomous periodic and damping perturbations by this new extended method and numerical simulations. The numerical results verify the correctness of the theoretical results and demonstrate that this extended method is simple and effective for studying the dynamics of such systems.

Many systems in various fields such as mechanical engineering, control science and electronics, inevitably contain non-smoothness and randomness. Thus, the classical Melnikov method, which is a powerful tool for analyzing chaos but only about the smooth vector field, needs to be developed urgently. At present, many some phased progress has been made on either deterministic discontinuous systems without random influences or the random systems without discontinuous influences. Few works combine two influencing factors. Recently, we [Li *et al.*, Chaos 32, 073119 (2022)] have extended the classical Melnikov method for homoclinic orbits to a class of hybrid piecewise-smooth systems with impulsive effect and noise excitation. Since the derivation process and form of homoclinic and heteroclinic Melnikov functions are different in non-smooth systems, we now extend the work of Li *et al.* [Chaos 32, 073119 (2022)] to the homoclinic case to the heteroclinic case.

I. INTRODUCTION

Many nonlinear systems both involve randomness or piecewise-smooth effects in multi-disciplinary fields, such as mechanics,[1,2] engineering application,[3] physiology,[4] an so on,[5,6] research methods and theories are constantly improving and developing with complexity of the derived structure. Additionally, scholars in the field of nonlinear dynamical systems have always shown great interest in the study of bifurcations[7,8] and chaotic dynamics.[9,10] For example, Faghani *et al.*[11] proposed some three-dimensional chaotic systems

with identical eigenvalues based on the general form of quadratic jerk systems and investigated their dynamics. Wei *et al.*[12] analyzed the bifurcation dynamics of a two-disk dynamo model with viscous friction and time delays. Exploring and studying bifurcations and chaotic behaviour in naturally occuring piecewise-smooth systems is also a key and important topic. Because of the limitation of relevant analytical methods, it is more difficult to identify clearly physical mechanisms of chaos arising in piecewise-smooth systems. In order to study such problems, it is, therefore, imperative to develop the classical Melnikov method[13–15] for predicing chaos in smooth systems to piecewise-smooth systems. The classical approach normally requires the vector field of the systems under investigation to be smooth, which limits its direct application to piecewise-smooth systems.

Recently, many scholars have developed the Melnikov method. Shi *et al.*[16] derived and validated the procedure for deriving the Melnikov function for plane discontinuous systems introduced by Kunze[17] for the first time in detail. Castro *et al.*[18] developed and considered a system with the pseudo-equilibrium point and discontinuity via the Melnikov method. Du *et al.*[19] discussed relevant homoclinic bifurcations for a type of inverted pendulum with external excitation and impact through the non-smooth Melnikov method. Battelli and Fečkan extended the previous results about the Melnikov method to high-dimensional systems by utilizing exponential dichotomy and variational technique in Refs. 20 and 21 and considered the sliding homoclinic case of this method in Ref. 22. These relevant results are summarized in Ref. 23. Li *et al.*[24] analyzed a planar Hamiltonian system which has a piecewise homoclinic orbit, investigated the homoclinic orbit under perturbations, and obtained a Melnikov function in a complete integral form. This optimized the previous results of Battelli and Fečkan to a certain extent, making those results more readily applicable. Following Granados *et al.*,[25] Li *et al.* obtained the Melnikov functions for homoclinic and heteroclinic bifurcations in two hybrid piecewise-smooth systems by describing the relevant impacting rule on a switching manifold by the reset map in Refs. 26 and 27. Furthermore, Li *et al.*[28,29] developed a non-smooth Melnikov theory for both theoretical and experimental applications. Tian *et al.* investigated chaos in non-smooth systems under the influence of two classes of jump discontinuities in Ref. 30 and multiple impulsive effects in Ref. 31 by extending the Melnikov method of homoclinic orbits, and extended the results about the homoclinic case to the heteroclinic case in Ref. 32. According to the results about global dynamics for a new bistable nonlinear oscillator in Ref. 33, Zheng *et al.*[34] derived a Melnikov function to analyze chaos in the homoclinic case of a hybrid piecewise-smooth system with impulse.

Since randomness exists everywhere in nature, it is necessary to consider the effects of random excitation on dynamical behaviours. At present, there are no simple zeros for Melnikov functions in sense of the mean. So the statistical properties of relevant random Melnikov functions are studied, and the random Melnikov method is derived to deal with this kind of problem. Bulsara *et al.*[35] derived a generalized Melnikov function for studying chaotic response under noise. Frey *et al.*[36] conducted a investigation about the influence of additive noise on near-integrable dynamic systems by extending the Melnikov method. Lin *et al.*[37] used the mean-square criterion for random Melnikov functions to analyze a Duffing oscillator with additive noise and harmonic excitation. Recently, this criterion has been further developed and utilized in dichotomous noise excitation[38] for bounded noise,[39] for random disordered periodic input,[40] and so on. Significantly, Liu *et al.*[41] extended the random Melnikov method to discontinuous systems and studied chaos in such systems, induced by random disordered periodic input. These results, obtained in Ref. 41, combined discontinuous and random effects to determine the new Melnikov function.

Many previous studies have focused on either deterministic, discontinuous systems without random effects or on random systems without discontinuities. There are few relevant studies that combine the two factors. Therefore, in view of the complexity and requirements of applications, it is important to develop the Melnikov theory that combines the two factors of noise and discontinuities. In addition, there are many differences between the heteroclinic and homoclinic cases, which may lead to different types of results. Thus, in view of Refs. 27, 34, and 41, our motivation in this work is to extend the classical Melnikov method for heteroclinic orbits to a class of hybrid piecewise-smooth systems with both impulsive effects and noise excitation. We here emphasize how our present work differs from that of Refs. 27, 34, and 41. (*i*) Our system considers noise excitation, while the systems studied in Refs. 34 and 27 have no randomness. (*ii*) Our system considers both impulsive effects and the reset map describing the impact rule, while both Refs. 27 and 34 consider only one of these factors, respectively. (*iii*) Our piecewise-smooth system considers three factors: the heteroclinic case, impulsive effects, and the reset map, describing the impact rule, while the system studied in Ref. 41 considers only two factors: randomness and the homoclinic case; other factors are not considered. (*iv*) The form of the Melnikov function we derive is different from that in Refs. 27, 34, and 41. However, when some conditions of our system are simplified our results can be reduced or transformed into theirs. Therefore, this work extends that of Refs. 27, 34, and 41.

The structure of this paper is as follows: In Sec. II, the relevant system under investigation is introduced. The random Melnikov process for the heteroclinic orbits about a class of hybrid piecewise-smooth systems with impulsive effect and noise excitation is derived, and the criteria for the onset of chaos with or without noise excitation are established. In Sec. III, the dynamics of a corresponding concrete example with and without noise excitation are investigated by both Melnikov-type function and numerical simulations. Finally, we draw our conclusions in Sec. IV.

II. MELNIKOV ANALYSIS

A. The hybrid piecewise-smooth system

In this section, we extend the procedure of Li *et al.*[1] for the homoclinic case to the heteroclinic case and divide $\mathbb{R}^2$ into three

zones: $\mathbb{R}^2 = S_1 \cup \Sigma_1 \cup S_2 \cup \Sigma_2 \cup S_3$, where

$$\Sigma_1 = \{(x,y) \in \mathbb{R}^2 \mid x = \beta\}, \Sigma_2 = \{(x,y) \in \mathbb{R}^2 \mid x = \alpha\},$$
$$S_1 = \{(x,y) \in \mathbb{R}^2 \mid \beta < x\}, S_2 = \{(x,y) \in \mathbb{R}^2 \mid \alpha < x < \beta\}, \quad (1)$$
$$S_3 = \{(x,y) \in \mathbb{R}^2 \mid x < \alpha\},$$

and α and β are two constants. We define $\Sigma_k = \Sigma_k^+ \cup \Sigma_k^- \cup \{0\}$, $(k = 1, 2)$, which corresponds to $y > 0$, $y < 0$, $y = 0$. We take the piecewise-smooth system with impulsive effect and noise excitation in $\mathbb{R}^2$ to be

$$\begin{cases} \begin{pmatrix} \dot{x} \\ \dot{y} \end{pmatrix} = JDH(x,y) + \varepsilon G(x,y,t), \\ \quad = \begin{cases} JDH_1(x,y) + \varepsilon G_1(x,y,t), & (x,y) \in S_1, \\ JDH_2(x,y) + \varepsilon G_2(x,y,t), & (x,y) \in S_2, \\ JDH_3(x,y) + \varepsilon G_3(x,y,t), & (x,y) \in S_3, \end{cases} \\ \Delta x \mid_{x=\alpha,\beta} = 0, \\ \Delta y \mid_{x=\alpha,\beta} \neq 0. \end{cases} \quad (2)$$

Here, $G_i(x,y,t) = f_i(x,y,t) + g_i(x,y)\xi(t)$ for $(x,y) \in \mathbb{R}^2$; $0 < \varepsilon \ll 1$; the Hamiltonian function is $H_i : \mathbb{R}^2 \to \mathbb{R}$; $f_i : \mathbb{R}^2 \times \mathbb{R} \to \mathbb{R}^2$ and $\hat{T}$-periodic in t; $g_i : \mathbb{R}^2 \to \mathbb{R}$ are all sufficiently differentiable in the corresponding region for $i = 1, 2,$ and 3. We let D denote $\left(\frac{\partial}{\partial x}, \frac{\partial}{\partial y}\right)^T$, $J = \begin{pmatrix} 0 & 1 \\ -1 & 0 \end{pmatrix}$, $JDH_i(x,y) = \begin{pmatrix} y \\ h_i(x) \end{pmatrix}$, $f_i(x,y,t) = \begin{pmatrix} 0 \\ f_{i1}(x,y,t) \end{pmatrix}$, and $g_i(x,y) = \begin{pmatrix} 0 \\ g_{i1}(x,y) \end{pmatrix}$.

The unit normal vector for Σ_1, Σ_2 is $\mathbf{n} = (1,0)$, $\left(\forall(\alpha,y) \in \Sigma_1, \forall(\beta,y) \in \Sigma_2\right)$.

We take $x^{\pm} \mid_{x=\alpha,\beta}$ to be right and left limits for x at $x = \alpha,\ \beta$, i.e.,

$$\Delta x \mid_{x=\alpha,\beta} = x^- \mid_{x=\alpha,\beta} - x^+ \mid_{x=\alpha,\beta}.$$

Similarly, we have $y^{\pm} \mid_{x=\alpha,\beta}$. Then, on the switching manifold Σ_1, we have

$$y^- \mid_{x=\beta} = (1 - \varepsilon\eta_1) a y^+ \mid_{x=\beta}, \quad (3)$$

where $(1 - \varepsilon\eta_1)a$ and a denote instantaneous changes of perturbed and unperturbed systems due to the impulsive effect on the switching manifold Σ_1, respectively.

We next define the reset map, describing the impact rule on Σ_2,

$$\begin{aligned} \eta_0 : \Sigma_2 \times \mathbb{R} &\to \Sigma_2 \\ (\alpha, y, \varepsilon) &\mapsto (\alpha, \eta_{0,\varepsilon}(y)), \end{aligned} \quad (4)$$

which satisfies $y \cdot \eta_{0,\varepsilon}(y) > 0$ for $y \neq 0$, $\eta_{0,0}(y) = y$, $\eta_0^{-1}(\alpha, y, \varepsilon) = (\alpha, \eta_{0,\varepsilon}^{-1}(y))$, and η_0^{-1} is the inverse map of η_0. We provide some useful notation to be used later: $\Pi_{x(y)}$ is defined through $\Pi_x(x,y) = x$ and $\Pi_y(x,y) = y$.

For the noise excitation, $\xi(t)$ is taken to be Gaussian white noise with

$$E\xi(t) = 0, E\xi(t)\xi(t+\tau) = \begin{cases} \infty & (\tau = 0) \\ 0 & (\tau \neq 0). \end{cases}$$

Its corresponding spectral density $S_\xi(\omega)$ is constant for all frequencies ω. By Refs. 36, 42, and 43, we approximate $\xi(t)$ by the sum of some harmonic functions with random phases and frequencies; this is required in the subsequent analysis for a random Melnikov process.

According to the above description of systems (2)–(4), $x = \alpha$ and $x = \beta$ are two switching manifolds for this system, which divides $\mathbb{R}^2 = S_1 \cup \Sigma_1 \cup S_2 \cup \Sigma_2 \cup S_3$ into three different regimes, with the dynamics of each S_i corresponding to a subsystem. We assume that a trajectory crosses Σ_2 at (x,y) before it enters another zone. The reset map describing the impact rule on Σ_2 is used and the trajectory jumps from (x,y) to $(x, \eta_{0,\varepsilon}(y))$ instantaneously. For the other switching manifold Σ_1, the trajectory receives the impulsive effect stimulation on Σ_1, thereby causing an instantaneous sudden change. Then, this trajectory jumps across the switching manifold Σ_1.

In the theoretical derivation part of this paper, we only consider a heteroclinic orbit in the upper half-plane and assume that the trajectory is counterclockwise without loss of generality. It should be noted that the results and derivation process for the case of considering the heteroclinic orbit in the lower half-plane and assuming the orbit is clockwise are similar to those in this paper, except for the representation symbols of corresponding positions, which is due to the symmetry between the two cases. Why the results corresponding to these two cases are the same will be given in detail in the remarks below. And other assumptions are as follows:

$\mathbf{L}_1$: For $\forall(\beta,y) \in \Sigma_1$ and $\forall(\alpha,y) \in \Sigma_2$, $[\mathbf{n} \cdot JDH_1(\beta,y)] \cdot [\mathbf{n} \cdot JDH_2(\beta,y)] > 0$, $[\mathbf{n} \cdot JDH_2(\alpha,y)] \cdot [\mathbf{n} \cdot JDH_3(\alpha,y)] > 0$.

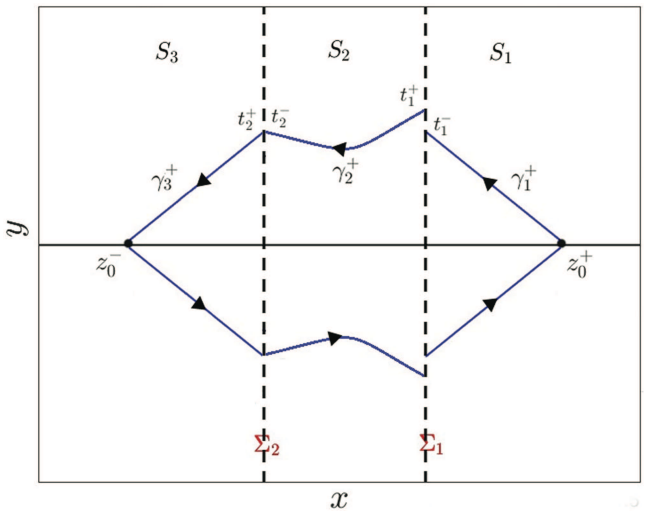

FIG. 1. The heteroclinic connection of systems (2)–(4) with $\varepsilon = 0$.

$\mathbf{L}_2$: As shown in Fig. 1, when $\varepsilon = 0$, systems (2)–(4) have two hyperbolic equilibria $z_0^+ = (x_0^+, y_0^+) \in S_1$ and $z_0^- = (x_0^-, y_0^-) \in S_3$. The upper heteroclinic orbit $\gamma^+(t)$ is

$$\gamma^+(t) = \begin{cases} \gamma_1^+(t) \in S_1, \ t \le t_1^-, \\ \gamma_2^+(t) \in S_2, \ t_1^+ \le t \le t_2^-, \\ \gamma_3^+(t) \in S_3, \ t_2^+ \le t, \end{cases} \tag{5}$$

where $t_1^\pm$ and $t_2^\pm$ mean the times when $\gamma^+(t)$ reaches or leaves the first and second switching manifolds Σ_1 and Σ_2, respectively, $t_1^\pm < t_2^\pm$. For the corresponding case where the lower half-plane heteroclinic orbit is considered and the orbit is assumed to be clockwise, the lower half-plane heteroclinic orbit should be expressed as $\gamma^-(t)$ accordingly, and the corresponding time also needs to be transformed into the corresponding representation. Then, for Fig. 1, we have

$$\begin{aligned} \gamma_1^+(t_1^-) &= [x_1^+(t_1^-), y_1^+(t_1^-)]^T = (\beta, y_1)^T \in \Sigma_1^+, \\ \gamma_2^+(t_1^+) &= [x_2^+(t_1^+), y_2^+(t_1^+)]^T = (\beta, y_2)^T \in \Sigma_1^+, \\ \gamma_2^+(t_2^-) &= [x_2^+(t_2^-), y_2^+(t_2^-)]^T = (\alpha, y_3)^T \in \Sigma_2^+, \\ \gamma_3^+(t_2^+) &= [x_3^+(t_1^+), y_3^+(t_2^+)]^T = (\alpha, y_3)^T \in \Sigma_2^+. \end{aligned} \tag{6}$$

B. The Melnikov-type function for system (2)–(4)

The Melnikov-type function for system (2)–(4) will be derived in this section. This analysis follows that for the homoclinic orbit in Ref. 1. In the light of construction of classical Melnikov functions,[14] without losing generality, we will study the following case, namely, the perturbed unstable and stable manifolds will be broken and will intersect transversely in the upper half-plane of S_2.

For $0 < \varepsilon \ll 1$, the perturbed unstable manifold is

$$q^u(t, t_0, \varepsilon) = \begin{cases} q^{u,1}(t, t_0, \varepsilon) = \gamma_1^+(t - t_0) + \varepsilon q_1^{u,1}(t, t_0) + O(\varepsilon^2), \ t \le t_{1,\varepsilon}^-, \\ q^{u,2}(t, t_0, \varepsilon) = \gamma_2^+(t - t_0) + \varepsilon q_1^{u,2}(t, t_0) + O(\varepsilon^2), \ t_{1,\varepsilon}^+ \le t \le t_0, \end{cases} \tag{7}$$

and the perturbed stable manifold is

$$q^s(t, t_0, \varepsilon) = \begin{cases} q^{s,2}(t, t_0, \varepsilon) = \gamma_2^+(t - t_0) + \varepsilon q_1^{s,2}(t, t_0) + O(\varepsilon^2), \ t_0 \le t \le t_{2,\varepsilon}^-, \\ q^{s,3}(t, t_0, \varepsilon) = \gamma_3^+(t - t_0) + \varepsilon q_1^{s,3}(t, t_0) + O(\varepsilon^2), \ t \ge t_{2,\varepsilon}^+, \end{cases} \tag{8}$$

where $t_{1,\varepsilon}^\pm$ and $t_{2,\varepsilon}^\pm$ mean the times when $q^{u(s)}(t, t_0, \varepsilon)$ either reach or leave the first and second switching manifolds Σ_1 and Σ_2, $t_{k,\varepsilon}^- = t_{k,\varepsilon}^+$ $(k = 1, 2)$, i.e.,

$$t_{1,\varepsilon}^\pm = t_1^\pm + t_0 + \varepsilon t_{1,1}^\pm + O(\varepsilon^2), \ t_{2,\varepsilon}^\pm = t_2^\pm + t_0 + \varepsilon t_{2,1}^\pm + O(\varepsilon^2), \tag{9}$$

$$q^{u(s),i}(t, t_0, \varepsilon) = [x^{u(s),i}(t, t_0, \varepsilon), \ y^{u(s),i}(t, t_0, \varepsilon)]^T, \ (i = 1, 2, 3), \tag{10}$$

$$q^{u,1}(t_{1,\varepsilon}^-, t_0, \varepsilon) \ne q^{u,2}(t_{1,\varepsilon}^+, t_0, \varepsilon), \ q^{s,2}(t_{2,\varepsilon}^-, t_0, \varepsilon) \ne q^{s,3}(t_{2,\varepsilon}^+, t_0, \varepsilon). \tag{11}$$

Then, $q_1^{u(s),i}(t, t_0)$ $(i = 1, 2, 3)$ are governed by

$$\dot{q}_1^{u(s),i}(t, t_0) = JD^2 H_i(\gamma(t - t_0)) \cdot q_1^{u(s),i}(t, t_0) + G_i(\gamma(t - t_0), t). \tag{12}$$

Following the classical approach of Ref. 14, we let

$$\Delta_\varepsilon^{u(s),i}(t, t_0) = \varepsilon JDH_i(\gamma(t - t_0)) \wedge q_1^{u(s),i}(t, t_0). \tag{13}$$

Differentiating (13) and using (12), we obtain

$$\dot{\Delta}_\varepsilon^{u(s),i}(t, t_0) = \varepsilon JDH_i(\gamma(t - t_0)) \wedge G_i(\gamma(t - t_0), t), \tag{14}$$

where $i = 1, 2, 3$, $\Delta_\varepsilon^{u,1}(-\infty, t_0) = \Delta_\varepsilon^{s,3}(+\infty, t_0) = 0$ since $JDH_1(x_0^+, y_0^+) = JDH_3(x_0^-, y_0^-) = 0$, and $q_1^{u(s),i}(t, t_0)$ are bounded. Then, the distance between $q^u(t_0, t_0, \varepsilon)$ and $q^s(t_0, t_0, \varepsilon)$ is

$$\begin{aligned} \Delta_\varepsilon(t_0) &= \Delta_\varepsilon^{u,2}(t_0, t_0) - \Delta_\varepsilon^{s,2}(t_0, t_0) + O(\varepsilon^2), \\ &= [\Delta_\varepsilon^{u,2}(t_0, t_0) - \Delta_\varepsilon^{u,2}(t_0 + t_1^+, t_0)] + [\Delta_\varepsilon^{u,2}(t_0 + t_1^+, t_0) - \Delta_\varepsilon^{u,1}(t_0 + t_1^-, t_0)] \\ &\quad + [\Delta_\varepsilon^{u,1}(t_0 + t_1^-, t_0) - \Delta_\varepsilon^{u,1}(-\infty, t_0)] + [\Delta_\varepsilon^{u,1}(-\infty, t_0) - \Delta_\varepsilon^{s,3}(+\infty, t_0)] \end{aligned}$$

$$
\begin{aligned}
&+ [\Delta_\varepsilon^{s,3}(+\infty, t_0) - \Delta_\varepsilon^{s,3}(t_0 + t_2^+, t_0)] + [\Delta_\varepsilon^{s,3}(t_0 + t_2^+, t_0) - \Delta_\varepsilon^{s,2}(t_0 + t_2^-, t_0)] \\
&+ [\Delta_\varepsilon^{s,2}(t_0 + t_2^-, t_0) - \Delta_\varepsilon^{s,2}(t_0, t_0)] + O(\varepsilon^2), \\
&= \varepsilon \int_{-\infty}^{+\infty} JDH(\gamma(t - t_0)) \wedge G(\gamma(t - t_0), t)dt + [\Delta_\varepsilon^{u,2}(t_0 + t_1^+, t_0) - \Delta_\varepsilon^{u,1}(t_0 + t_1^-, t_0)] \\
&+ [\Delta_\varepsilon^{s,3}(t_0 + t_2^+, t_0) - \Delta_\varepsilon^{s,2}(t_0 + t_2^-, t_0)] + O(\varepsilon^2),
\end{aligned} \tag{15}
$$

where

$$
- \Delta_\varepsilon^{s,3}(t_0 + t_2^+, t_0) = \varepsilon \int_{t_2^+ + t_0}^{+\infty} JDH_3(\gamma(t - t_0)) \wedge G_3(\gamma(t - t_0), t)dt. \tag{16}
$$

First, we calculate $\Delta_\varepsilon^{s,2}(t_0 + t_2^-, t_0)$. Then, the following theorem will be proved:

Theorem II.1.

$$
\Delta_\varepsilon^{s,2}(t_0 + t_2^-, t_0) = \varepsilon \dot{\gamma}_2^+(t_2^-) \wedge \frac{\partial \eta_0^{-1}(\gamma(t_2^+), 0)}{\partial \varepsilon} + \frac{\boldsymbol{n}(\gamma(t_2^+)) \cdot D^* \eta_0^{-1}(\gamma(t_2^+), 0)\dot{\gamma}_2^+(t_2^-)}{\boldsymbol{n}(\gamma(t_2^+)) \cdot \dot{\gamma}_3^+(t_2^+)} \times \Delta_\varepsilon^{s,3}(t_0 + t_2^+, t_0), \tag{17}
$$

where

$$
D\eta_0^{-1}(\gamma(t_2^+), 0) = \begin{pmatrix} 0 & 0 \\ 0 & \frac{\partial \eta_{0,0}^{-1}}{\partial y}(\Pi_\gamma \gamma(t_2^+)) \end{pmatrix},
$$

and $D^* \eta_0^{-1}(\gamma(t_2^+), 0)$ *is the adjoint of* $D\eta_0^{-1}(\gamma(t_2^+), 0)$.

Proof. For $t \in (t_0, t_{2,\varepsilon}^-)$, we have

$$
\eta_0^{-1}(q^{s,3}(t_{2,\varepsilon}^+, t_0, \varepsilon), \varepsilon) = q^{s,2}(t, t_0, \varepsilon) + \int_t^{t_{2,\varepsilon}^-} JDH_2(q^{s,2}(s, t_0, \varepsilon)) + \varepsilon G_2(q^{s,2}(s, t_0, \varepsilon))ds, \tag{18}
$$

so that

$$
q^{s,2}(t, t_0, \varepsilon) = \eta_0^{-1}(q^{s,3}(t_{2,\varepsilon}^+, t_0, \varepsilon), \varepsilon) + \int_{t_{2,\varepsilon}^-}^t JDH_2(q^{s,2}(s, t_0, \varepsilon)) + \varepsilon G_2(q^{s,2}(s, t_0, \varepsilon))ds. \tag{19}
$$

Differentiating (19) with respect to ε, substituting $t_2^- + t_0$ for t and 0 into ε, we get

$$
\begin{aligned}
q_1^{s,2}(t_0 + t_2^-, t_0) = &\frac{\partial \eta_0^{-1}(\gamma(t_2^+), 0)}{\partial \varepsilon} + D\eta_0^{-1}(\gamma(t_2^+), 0) q_1^{s,3}(t_0 + t_2^+, t_0) \\
&+ [D\eta_0^{-1}(\gamma(t_2^+), 0)\dot{\gamma}_3^+(t_2^+) - \dot{\gamma}_2^+(t_2^-)] \left. \frac{dt_{2,\varepsilon}^-}{d\varepsilon} \right|_{\varepsilon=0}.
\end{aligned} \tag{20}
$$

Since $q^{s,3}(t_{2,\varepsilon}^+, t_0, \varepsilon) \in \Sigma_2^+$, we obtain

$$
\Pi_x(q^{s,3}(t_{2,\varepsilon}^+, t_0, \varepsilon)) = \alpha. \tag{21}
$$

Differentiating (21) about ε, with $t_{2,\varepsilon}^- = t_{2,\varepsilon}^+$, evaluating at $\varepsilon = 0$, we obtain

$$
\left. \frac{dt_{2,\varepsilon}^-}{d\varepsilon} \right|_{\varepsilon=0} = -\frac{\mathbf{n}(\gamma(t_2^+)) \cdot q_1^{s,3}(t_0 + t_2^+, t_0)}{\mathbf{n}(\gamma(t_2^+)) \cdot \dot{\gamma}_3^+(t_2^+)}. \tag{22}
$$

□

Substituting (22) and (20) into (13), we derive (17) as follows:

$$\begin{aligned}\Delta_{\varepsilon}^{s,2}(t_0+t_2^-,t_0) &= \varepsilon JDH_2(\gamma(t_2^-))\wedge q_1^{s,2}(t_0+t_2^-,t_0)\\ &= \varepsilon\dot\gamma_2^+(t_2^-)\wedge\left\{\frac{\partial\eta_0^{-1}(\gamma(t_2^+),0)}{\partial\varepsilon}+\left[D\eta_0^{-1}(\gamma(t_2^+),0)\right.\right.\\ &\quad\left.\left.+\frac{[\dot\gamma_2^+(t_2^-)-D\eta_0^{-1}(\gamma(t_2^+),0)\dot\gamma_3^+(t_2^+)]\mathbf{n}(\gamma(t_2^+))}{\mathbf{n}(\gamma(t_2^+))\cdot\dot\gamma_3^+(t_2^+)}\right]q_1^{s,3}(t_0+t_2^+,t_0)\right\}\\ &= \varepsilon\dot\gamma_2^+(t_2^-)\wedge\frac{\partial\eta_0^{-1}(\gamma(t_2^+),0)}{\partial\varepsilon}+\varepsilon\frac{\mathbf{n}(\gamma(t_2^+))\cdot D^*\eta_0^{-1}(\gamma(t_2^+),0)\dot\gamma_2^+(t_2^-)}{\mathbf{n}(\gamma(t_2^+))\cdot\dot\gamma_3^+(t_2^+)}\\ &\quad\times\dot\gamma_3^+(t_2^+)\wedge q_1^{s,3}(t_0+t_2^+,t_0)\\ &= \varepsilon\dot\gamma_2^+(t_2^-)\wedge\frac{\partial\eta_0^{-1}(\gamma(t_2^+),0)}{\partial\varepsilon}+\frac{\mathbf{n}(\gamma(t_2^+))\cdot D^*\eta_0^{-1}(\gamma(t_2^+),0)\dot\gamma_2^+(t_2^-)}{\mathbf{n}(\gamma(t_2^+))\cdot\dot\gamma_3^+(t_2^+)}\\ &\quad\times\Delta_{\varepsilon}^{s,3}(t_0+t_2^+,t_0).\end{aligned}\tag{23}$$

Second, we calculate $\Delta_{\varepsilon}^{u,2}(t_0+t_1^+,t_0)-\Delta_{\varepsilon}^{u,1}(t_0+t_1^-,t_0)$.
By Ref. 32, we have

$$\Delta_{\varepsilon}^{u,2}(t_0+t_1^+,t_0)-\Delta_{\varepsilon}^{u,1}(t_0+t_1^-,t_0)=\varepsilon(A-B),\tag{24}$$

where

$$A=y_2^+(t_1^+)y_1^{u,2}(t_1^++t_0,t_0)-h_2(x_2^+(t_1^+))x_1^{u,2}(t_1^++t_0,t_0),\tag{25}$$

$$B=y_1^+(t_1^-)y_1^{u,1}(t_1^-+t_0,t_0)-h_1(x_1^+(t_1^-))x_1^{u,1}(t_1^-+t_0,t_0).\tag{26}$$

From Refs. 31 and 32, we know that the perturbed solution $q^{u,2}(t_{1,\varepsilon}^+,t_0,\varepsilon)$ takes the following form

$$q^{u,2}(t_{1,\varepsilon}^+,t_0,\varepsilon)=q^{u,2}(t_1^++t_0,t_0,\varepsilon)+\varepsilon t_1^+JDH_2(q^{u,2}(t_1^++t_0,t_0,\varepsilon)).\tag{27}$$

From (7), (8), and (27), we obtain

$$t_1^+=-\frac{x_1^{u,2}(t_1^++t_0,t_0)}{y_2^+(t_1^+)}+O(\varepsilon),\tag{28}$$

$$y^{u,2}(t_{1,\varepsilon}^+,t_0,\varepsilon)=y_2^+(t_1^+)+\varepsilon t_1^+h_2(x_2^+(t_1^+))+\varepsilon y_1^{u,2}(t_1^++t_0,t_0)+O(\varepsilon^2),\tag{29}$$

and substituting (28) into (29) gives

$$y^{u,2}(t_{1,\varepsilon}^+,t_0,\varepsilon)=y_2^+(t_1^+)-\varepsilon\frac{x_1^{u,2}(t_1^++t_0,t_0)}{y_2^+(t_1^+)}h_2(x_2^+(t_1^+))+\varepsilon y_1^{u,2}(t_1^++t_0,t_0)+O(\varepsilon^2).\tag{30}$$

Similarly,

$$y^{u,1}(t_{1,\varepsilon}^-,t_0,\varepsilon)=y_1^+(t_1^-)-\varepsilon\frac{x_1^{u,1}(t_1^-+t_0,t_0)}{y_1^+(t_1^-)}h_1(x_1^+(t_1^-))+\varepsilon y_1^{u,1}(t_1^-+t_0,t_0)+O(\varepsilon^2).\tag{31}$$

From (3), we obtain

$$\begin{aligned}y_2^+(t_1^+)&=ay_1^+(t_1^-),\\ y^{u,2}(t_{1,\varepsilon}^+,t_0,\varepsilon)&=(1-\varepsilon\eta_1)ay^{u,1}(t_{1,\varepsilon}^-,t_0,\varepsilon).\end{aligned}\tag{32}$$

Thus,

$$y_1^{u,2}(t_1^++t_0,t_0)-\frac{x_1^{u,2}(t_1^++t_0,t_0)}{y_2^+(t_1^+)}h_2(x_2^+(t_1^+))=ay_1^{u,1}(t_1^-+t_0,t_0)-a\frac{x_1^{u,1}(t_1^-+t_0,t_0)}{y_1^+(t_1^-)}h_1(x_1^+(t_1^-))-\eta_1ay_1^+(t_1^-)+O(\varepsilon),\tag{33}$$

namely,

$$\begin{aligned} A &= y_2^+(t_1^+)y_1^{u,2}(t_1^+ + t_0, t_0) - x_1^{u,2}(t_1^+ + t_0, t_0)h_2(x_2^+(t_1^+)) \\ &= a^2 y_1^+(t_1^-)y_1^{u,1}(t_1^- + t_0, t_0) - a^2 x_1^{u,1}(t_1^- + t_0, t_0)h_1(x_1^+(t_1^-)) - \eta_1 a^2 [y_1^+(t_1^-)]^2 + O(\varepsilon) \\ &= a^2 B - \eta_1 a^2 [y_1^+(t_1^-)]^2 + O(\varepsilon) \end{aligned} \tag{34}$$

and

$$y_1^+(-\infty) = 0,\ h_1(x_1^+(-\infty)) = 0.$$

Therefore,

$$\begin{aligned} B &= [y_1^+(t_1^-)y_1^{u,1}(t_1^- + t_0, t_0) - h_1(x_1^+(t_1^-))x_1^{u,1}(t_1^- + t_0, t_0)] \\ &\quad - [y_1^+(-\infty)y_1^{u,1}(-\infty, t_0) - h_1(x_1^+(-\infty))x_1^{u,1}(-\infty, t_0)] \\ &= \int_{-\infty}^{t_1^- + t_0} JDH_1(\gamma_1^+(t - t_0)) \wedge G_1(\gamma_1^+(t - t_0), t)dt. \end{aligned} \tag{35}$$

According to Ref. 31, we have

$$(y_1^+(t_1^-))^2 = 2\int_{x_0^+}^{\beta} h_1(x)dx. \tag{36}$$

Therefore,

$$A - B = (a^2 - 1)\int_{-\infty}^{t_1^- + t_0} JDH_1(\gamma_1^+(t - t_0)) \wedge G_1(\gamma_1^+(t - t_0), t)dt - 2\eta_1 a^2 \int_{x_0^+}^{\beta} h_1(x)dx. \tag{37}$$

Substituting (16), (17), (24), and (37) into (15) and performing the appropriate variable substitutions, we obtain the following non-smooth Melnikov-type function for a random process: it contains both a deterministic and a random component,

$$M(t_0) = M_d(t_0) + M_r(t_0). \tag{38}$$

The deterministic term is

$$\begin{aligned} M_d(t_0) &= -\dot{\gamma}_2^+(t_2^-) \wedge \frac{\partial \eta_0^{-1}(\gamma(t_2^+), 0)}{\partial \varepsilon} + a^2 \int_{-\infty}^{t_1^-} JDH_1(\gamma_1^+(t)) \wedge f_1(\gamma_1^+(t), t + t_0)dt \\ &\quad + \int_{t_1^+}^{t_2^-} JDH_2(\gamma_2^+(t)) \wedge f_2(\gamma_2^+(t), t + t_0)dt - 2\eta_1 a^2 \int_{x_0^+}^{\beta} h_1(x)dx \\ &\quad + \frac{\mathbf{n}(\gamma(t_2^+)) \cdot D^* \eta_0^{-1}(\gamma(t_2^+), 0)\dot{\gamma}_2^+(t_2^-)}{\mathbf{n}(\gamma(t_2^+)) \cdot \dot{\gamma}_3^+(t_2^+)} \times \int_{t_2^+}^{+\infty} JDH_3(\gamma_3^+(t)) \wedge f_3(\gamma_3^+(t), t + t_0)dt, \end{aligned} \tag{39}$$

while the random term is

$$\begin{aligned} M_r(t_0) &= a^2 \int_{-\infty}^{t_1^-} JDH_1(\gamma_1^+(t)) \wedge g_1(\gamma_1^+(t))\xi(t + t_0)dt + \int_{t_1^+}^{t_2^-} JDH_2(\gamma_2^+(t)) \wedge g_2(\gamma_2^+(t))\xi(t + t_0)dt \\ &\quad + \frac{\mathbf{n}(\gamma(t_2^+)) \cdot D^* \eta_0^{-1}(\gamma(t_2^+), 0)\dot{\gamma}_2^+(t_2^-)}{\mathbf{n}(\gamma(t_2^+)) \cdot \dot{\gamma}_3^+(t_2^+)} \times \int_{t_2^+}^{+\infty} JDH_3(\gamma_3^+(t)) \wedge g_3(\gamma_3^+(t))\xi(t + t_0)dt. \end{aligned} \tag{40}$$

The random part of $M(t_0)$ is treated statistically,[41] and so $M_r(t_0)$ can be rewritten as in the convolution form,

$$M_r(t_0) = l(t) * \xi(t), \tag{41}$$

where

$$l(t) = \begin{cases} a^2 \left[JDH_1(\gamma_1^+(t)) \wedge g_1(\gamma_1^+(t))\right],\ t \le t_1^-, \\ JDH_2(\gamma_2^+(t)) \wedge g_2(\gamma_2^+(t)),\ t_1^+ \le t \le t_2^-, \\ \dfrac{\mathbf{n}(\gamma(t_2^+)) \cdot D^* \eta_0^{-1}(\gamma(t_2^+), 0)\dot{\gamma}_2^+(t_2^-)}{\mathbf{n}(\gamma(t_2^+)) \cdot \dot{\gamma}_3^+(t_2^+)} \times [JDH_3(\gamma_3^+(t)) \wedge g_3(\gamma_3^+(t))],\ t \ge t_2^+. \end{cases} \tag{42}$$

When $\xi(t)$ is the noise input of system, we regard $l(t)$ as the impulse response for the system, with relevant frequency response function,

$$H_0(\omega) = \int_{-\infty}^{+\infty} l(t)e^{-j\omega t}dt. \tag{43}$$

Then,

$$E[M(t_0)] = M_d, \tag{44}$$

where $E[\cdot]$ is the expectation and the variance of $M_r(t_0)$ is

$$\begin{aligned}\sigma_r^2 &= E\left[(M_r(t_0))^2\right] - [E[M_r(t_0)]]^2 \\ &= \int_{-\infty}^{+\infty} |H_0(\omega)|^2 S_\xi(\omega)d\omega.\end{aligned} \tag{45}$$

The corresponding standard deviation is σ_r, which implies that $M(t_0)$ varies between $M_d - \sigma_r$ and $M_d + \sigma_r$.

According to the above analysis, and based on Refs. 15, 37, and 41, we obtain the following theorem:

Theorem II.2.

(i) *If $M_d(t_0) > 0$, $M(t_0)$ has no simple zeros for t_0 in both the mean and the mean-square senses.*

(ii) *If $M_d(t_0) = 0$, $M(t_0)$ has no simple zeros for t_0 in the mean-square sense, but it has simple zeros for t_0 under the mean sense if*

$$M_d(t_0) = 0. \tag{46}$$

(iii) *If $M_d(t_0) < 0$, $M(t_0)$ has no simple zeros for t_0 in the mean sense, but it has simple zeros for t_0 in the mean-square sense if*

$$M_d^2(t_0) = \sigma_r^2. \tag{47}$$

Remark 1. When generalized Melnikov funcion (38) has simple zeros in the statistical sense, the stable manifold of systems (2)–(4) intersects with the unstable manifold transversally, which means existence of chaos in such systems. Moreover, condition (46) is also the condition for chaos in the deterministic system without noise in systems (2)–(4).

Remark 2. The formula obtained by changing $\gamma^+(t)$ in (38) to the corresponding $\gamma^-(t)$ and transforming the corresponding time into corresponding representation is the corresponding Melnikov function obtained by considering the case where the lower half-plane heteroclinic orbit is studied and the trajectory is assumed to be clockwise. This is why, as mentioned above, the Melnikov functions obtained in these two cases are similar due to the existence of symmetry. Namely, the problem studied by considering the counterclockwise heteroclinic orbit in the upper half-plane is symmetrically the same as the problem studied by considering the clockwise heteroclinic orbit in the lower half-plane. Specifically, for the case of counterclockwise heteroclinic orbit in the upper half-plane with counterclockwise orbits, the heteroclinic orbit connecting the hyperbolic equilibrium z_0^+ to another hyperbolic equilibrium z_0^- in counterclockwise direction transversally jumps across the first switching manifold Σ_1 by impulsive effect and crosses the second switching manifold Σ_2 continuously, then the perturbed unstable and stable manifolds will be broken and will intersect transversely in the upper half-plane of S_2. For the case of the heteroclinic orbit in the lower half-plane and assuming the orbit is clockwise, the heteroclinic orbit connecting the hyperbolic equilibrium z_0^+ to another hyperbolic equilibrium z_0^- in the clockwise direction transversally jumps across the first switching manifold Σ_1 by an impulsive effect and crosses the second switching manifold Σ_2 continuously, then considering the perturbed unstable and stable manifolds will be broken and will intersect transversely in the lower half-plane of S_2. For these two cases, the starting and ending equilibrium points of the heteroclinic orbit, the sequence of the heteroclinic orbit crossing the switching manifolds, the external effects received by the heteroclinic orbit on each switching manifold, and the zone S_2 where the heteroclinic orbit is broken and intersected transversely are all the same. These similarities make the analysis and derivation process of the two cases similar and the results obtained are the same.

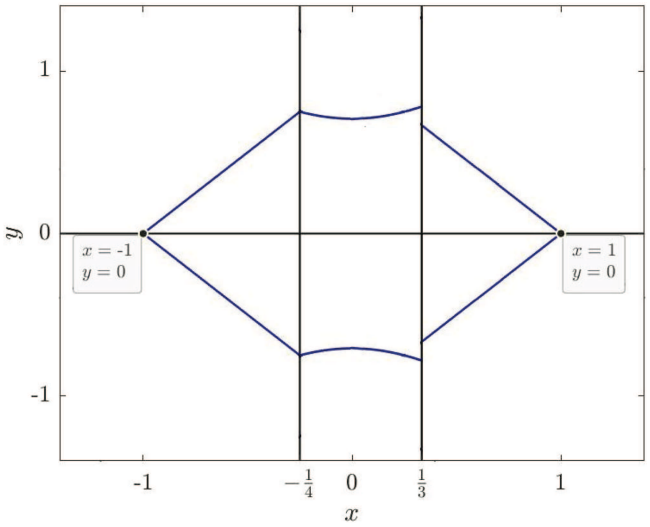

FIG. 2. The piecewise heteroclinic solution of the system (48)–(50) for $\varepsilon = 0$.

Remark 3. If $a = 1$, $\eta_1 = 0$, $\eta_0(\alpha, y, \varepsilon) = (\alpha, y)$, $t_1^+ = t_2^-$, systems (2)–(4) reduce to a piecewise-smooth system with noise under the assumption that the unperturbed system has heteroclinic orbits, crossing only one switching manifold. Then, $M(t_0)$ in (38) can be reduced to the heteroclinic case corresponding to $M(t_0)$ in Ref. 41. A further difference is that $\xi(t)$ has different meanings for Gaussian white noise excitation and for a random disordered periodical input.

Remark 4. If $\eta_0(\alpha, y, \varepsilon) = (\alpha, y)$, $g_i = 0$ $(i = 1, 2, 3)$, systems (2)–(4) reduce to a piecewise-smooth system with a pair of heteroclinic orbits jumping across only one switching manifold by impulse and crossing the other one continuously. Then, $M(t_0)$ in (38) reduces to the heteroclinic case corresponding to $M(t_0)$ in Ref. 34.

Remark 5. If $a = 1$, $\eta_1 = 0$, $g_i = 0$ $(i = 1, 2, 3)$, then the inclusion of an additional impact rule on Σ_1 where $\eta_0^* : (\beta, y, \varepsilon)$

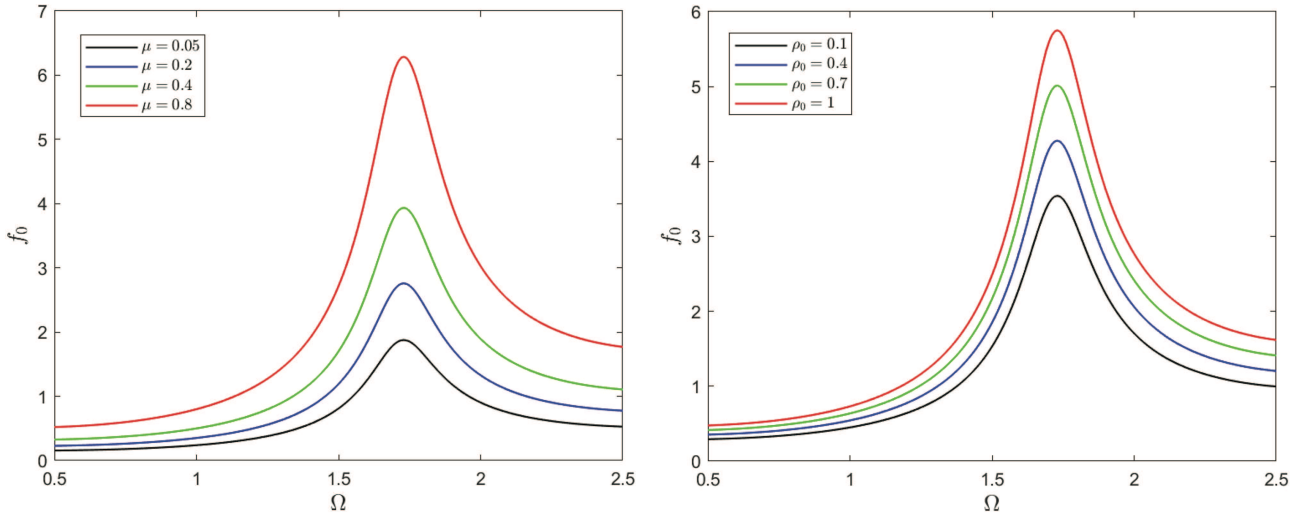

FIG. 3. The chaotic thresholds of systems (48)–(50) without noise excitation ($\delta = 0$) for different (a): μ, i.e., $\mu = 0.05,\ 0.2,\ 0.4,$ and 0.8 and (b): ρ_0, i.e., $\rho_0 = 0.1,\ 0.4,\ 0.7,$ and 1 in the (Ω, f_0) plane.

$\mapsto (\beta, \eta^*_{0,\varepsilon}(y))$ reduces systems (2)–(4) to the system studied in Ref. 27.

This work is, therefore, an extension of Refs. 27, 34, and 41. The above results are now applied to a specific piecewise-smooth system with impulsive effect and noise excitation.

III. APPLICATION AND NUMERICAL SIMULATIONS

We investigate the following system:

$$\begin{cases} \begin{cases} \dot{x} = y, \\ \dot{y} = x + 1 + \varepsilon\left[-\mu y + f_0 \cos\Omega t + \delta\xi(t)\right], \end{cases} & x < -\frac{1}{4}, \\ \begin{cases} \dot{x} = y, \\ \dot{y} = x + \varepsilon\left[-\mu y + f_0 \cos\Omega t + \delta\xi(t)\right], \end{cases} & -\frac{1}{4} < x < \frac{1}{3}, \\ \begin{cases} \dot{x} = y, \\ \dot{y} = x - 1 + \varepsilon\left[-\mu y + f_0 \cos\Omega t + \delta\xi(t)\right], \end{cases} & x > \frac{1}{3}, \\ \Delta x \mid_{x=\frac{1}{3},-\frac{1}{4}} = 0, \\ \Delta y \mid_{x=\frac{1}{3},-\frac{1}{4}} \neq 0, \end{cases} \tag{48}$$

where $0 < \varepsilon \ll 1$, μ is a damping coefficient, f_0 is periodic excitation coefficient, Ω is frequency, $\xi(t)$ means a Gaussian white noise, and δ means noise intensity. On the switching manifold $x = \frac{1}{3}$:

$$y^- \mid_{x=\frac{1}{3}} = \frac{\sqrt{22}}{4}(1 - \varepsilon\eta_1)y^+ \mid_{x=\frac{1}{3}}. \tag{49}$$

The reset map on the switching manifold $x = -\frac{1}{4}$ is

$$\eta_0 : (-\frac{1}{4}, y, \varepsilon) \mapsto \left(-\frac{1}{4}, \frac{y}{1-\varepsilon\rho_0 y}\right), \tag{50}$$

where ρ_0 is a positive parameter and

$$\eta_0^{-1} : (-\frac{1}{4}, y, \varepsilon) \mapsto \left(-\frac{1}{4}, \frac{y}{1+\varepsilon\rho_0 y}\right). \tag{51}$$

And

$$H(x,y) = \begin{cases} H_1(x,y) = \frac{1}{2}y^2 - \frac{1}{2}x^2 - x + \frac{1}{4}, & x < -\frac{1}{4}, \\ H_2(x,y) = \frac{1}{2}y^2 - \frac{1}{2}x^2 + \frac{1}{2}, & -\frac{1}{4} < x < \frac{1}{3}, \\ H_3(x,y) = \frac{1}{2}y^2 - \frac{1}{2}x^2 + x + \frac{1}{4}, & x > \frac{1}{3}. \end{cases} \tag{52}$$

The equilibria of the unperturbed system (48)–(50), i.e., $\varepsilon = 0$, are a center $(0,0)$ and two saddles $(\pm 1, 0)$. As shown in Fig. 2, the piecewise heteroclinic solution connecting $(1,0)$ to $(-1,0)$ in the clockwise direction is as follows. The following relevant analysis on example systems (48)–(50) corresponds to another case of considering the heteroclinic orbit in the lower half-plane and assuming the orbit is clockwise as described in **Remark 2**. The lower half-plane heteroclinic orbit is expressed as $\gamma^-(t)$, and the corresponding time should be transformed into corresponding representation. Here, for convenience, in this case, the times of reaching and leaving at first and second switching manifolds $x = \frac{1}{3}$ and $-\frac{1}{4}$ in the lower half-plane are still represented by $t_1^{\pm}$ and $t_2^{\pm}$,

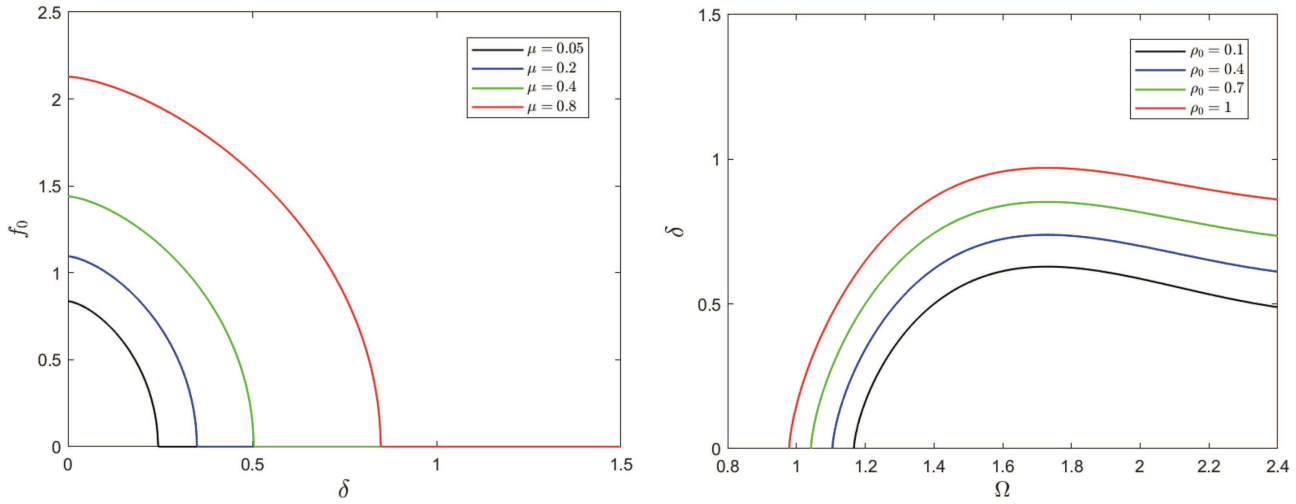

FIG. 4. The chaotic thresholds of systems (48)–(50) for different (a): μ, i.e., $\mu = 0.05,\ 0.2,\ 0.4,$ and 0.8 in the (δ, f_0) plane and (b): ρ_0, i.e., $\rho_0 = 0.1,\ 0.4,\ 0.7,$ and 1 in the (Ω, δ) plane.

$$\gamma^-(t) = \begin{cases} \left(-\frac{1}{2}\exp(t-t_a)+1, -\frac{1}{2}\exp(t-t_a)\right), & t \le t_1^-, \\ \left(\frac{\sqrt{2}}{4}(\exp(-t+t_b)-\exp(t-t_b)), -\frac{\sqrt{2}}{4}(\exp(t-t_b)+\exp(-t+t_b))\right), & t_1^+ \le t \le t_2^-, \\ \left(\frac{1}{2}\exp(t_c-t)-1, -\frac{1}{2}\exp(t_c-t)\right), & t \ge t_2^+, \end{cases} \tag{53}$$

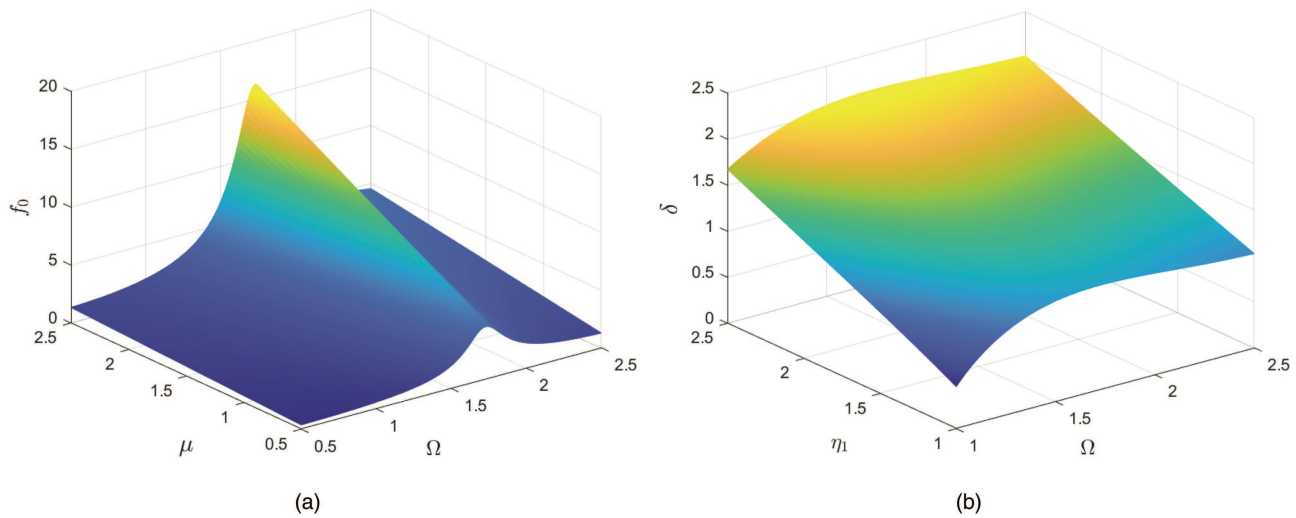

FIG. 5. The critical surface of systems (48)–(50) (a): without noise excitation ($\delta = 0,\ \rho_0 = 0.5$) in (Ω, μ, f_0) space and (b): with $\rho_0 = 0.1,\ \mu = 0.9,\ f_0 = 1$ in (Ω, η_1, δ) space.

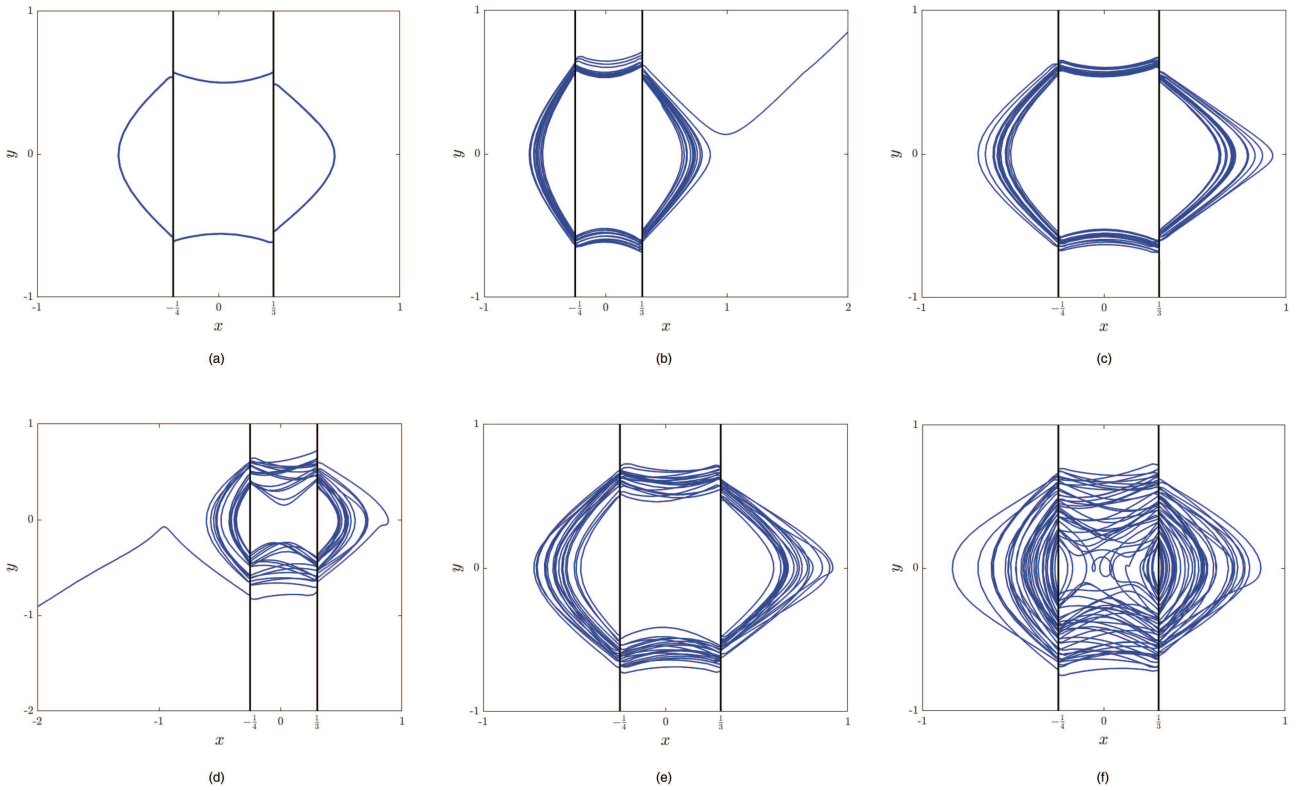

FIG. 6. The phase portraits of systems (48)–(50) without noise excitation ($\delta = 0$, $\varepsilon = 0.01$, $\mu = 0.08$, $\Omega = 1.6$, $\eta_1 = 0.1$, and $\rho_0 = 0.9$) for different f_0, (a) $f_0 = 1.2$, (b) $f_0 = 3$, (c) $f_0 = 3.5$, (d) $f_0 = 6.4$, (e) $f_0 = 8$, and (f) $f_0 = 16$.

where $t_a = 2\ln\frac{3}{2}$, $t_b = \ln(\sqrt{2}+\sqrt{11})$, $t_c = \ln\left[\frac{3\sqrt{2}(\sqrt{2}+\sqrt{11})}{2}\right]$, $t_1^{\pm} = \ln 3$, and $t_2^{\pm} = \ln[\sqrt{2}(\sqrt{2}+\sqrt{11})]$.

From (51)–(53), and according to the corresponding case of the formula (38) as described in **Remark 2**, we obtain the following non-smooth Melnikov-type function corresponding to systems (48)–(50) through calculation,

$$M(t_0) = -\rho_0 y_3^3 - \mu A + f_0\sqrt{B_1^2 + B_2^2}\sin(\Omega t_0 + \phi) - \frac{11}{18}\eta_1 + \int_{-\infty}^{+\infty} l(t)\xi(t+t_0)dt, \tag{54}$$

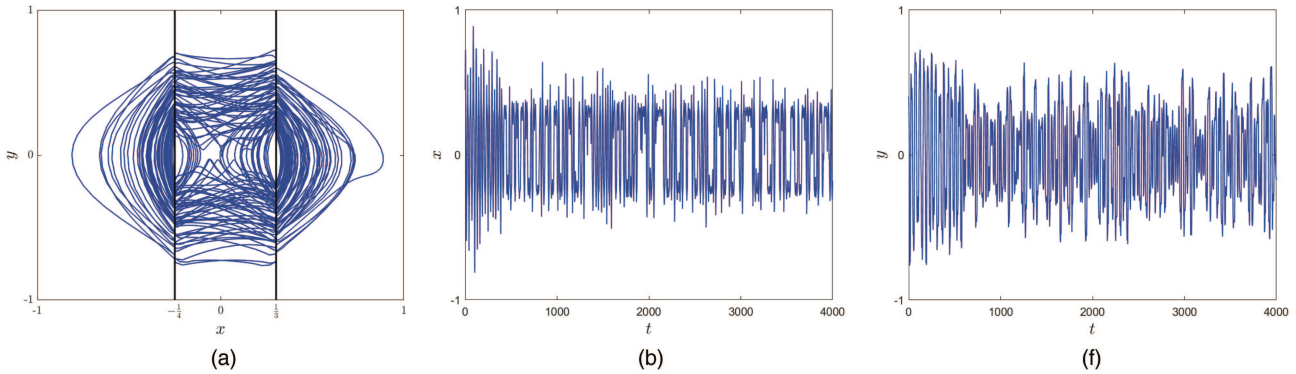

FIG. 7. The phase portraits and time series of systems (48)–(50) without noise excitation ($\delta = 0$, $\varepsilon = 0.01$, $\mu = 0.08$, $\Omega = 1.6$, $\eta_1 = 0.1$, and $\rho_0 = 0.9$) for $f_0 = 18.5$.

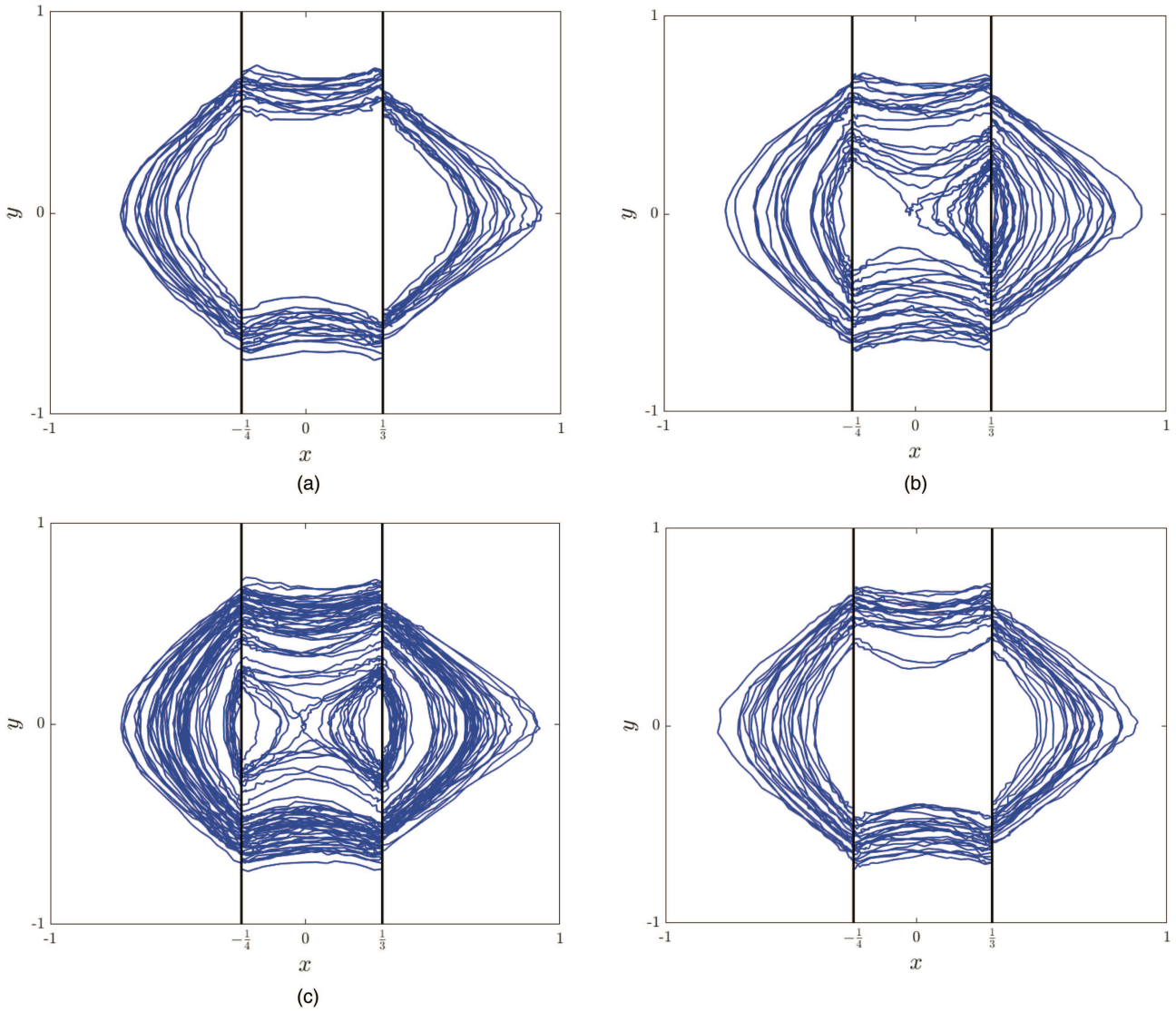

FIG. 8. The phase portraits of systems (48)–(50) with $\varepsilon = 0.01$, $\mu = 0.08$, $\Omega = 1.6$, $\eta_1 = 0.1$, and $\rho_0 = 0.9$ for $f_0 = 8$ and different δ: (a) $\delta = 0.000\,005$, (b) $\delta = 0.1$, (c) $\delta = 2$, and (d) $\delta = 5$.

where

$$a = \frac{\sqrt{22}}{4},\ \tan(\phi) = \frac{B_2}{B_1},$$

$$A = \frac{\sqrt{11}\left(\sqrt{2}+\sqrt{11}\right)}{36} + \frac{2\ln\left[\frac{\sqrt{2}(\sqrt{2}+\sqrt{11})}{3}\right]+3}{8},$$

$$B_1 = \frac{1}{4(\Omega^2+1)}\left\{(3a^2+1)\cos(\Omega t_1^{\pm}) + 3\cos(\Omega t_2^{\pm}) + \Omega[(3a^2-3)\sin(\Omega t_1^{\pm}) - (3-2\sqrt{2})\sin(\Omega t_2^{\pm})]\right\},$$

$$B_2 = \frac{1}{4(\Omega^2+1)}\left\{(3a^2+1)\sin(\Omega t_1^{\pm}) + 3\sin(\Omega t_2^{\pm}) + \Omega[(3a^2+3)\cos(\Omega t_1^{\pm}) + (3-2\sqrt{2})\cos(\Omega t_2^{\pm})]\right\}, \quad (55)$$

and the impulse response function $l(t)$ is

$$l(t) = \begin{cases} l_1(t) = -\dfrac{\delta a^2}{2}\exp(t-t_a),\ t \le t_1^-, \\ l_2(t) = -\dfrac{\sqrt{2}\delta}{4}(\exp(t-t_b) + \exp(-t+t_b)),\ t_1^+ \le t \le t_2^-, \\ l_3(t) = -\dfrac{\delta}{2}\exp(t_c - t),\ t \ge t_2^+. \end{cases} \quad (56)$$

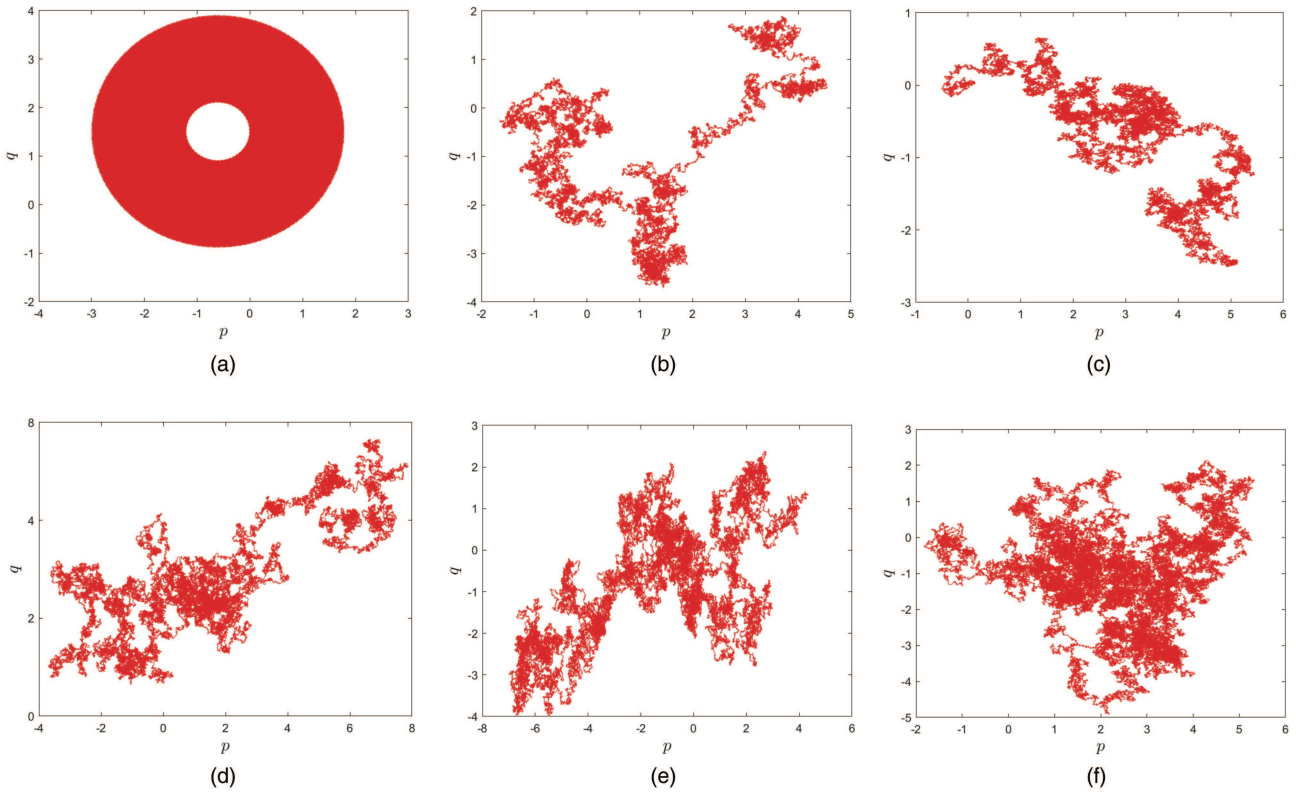

FIG. 9. The phase portraits of systems (48)–(50) without noise excitation ($\delta = 0$, $\varepsilon = 0.01$, $\mu = 0.08$, $\Omega = 1.6$, $\eta_1 = 0.1$, and $\rho_0 = 0.9$) in the new coordinates (p, q) for different f_0: (a) $f_0 = 1.2$, (b) $f_0 = 3$, (c) $f_0 = 3.5$, (d) $f_0 = 6.4$, (e) $f_0 = 8$, and (f) $f_0 = 16$.

According to **Theorem 2.1**, we have the following two cases:

Case A: no noise excitation

In the absence of noise, $M(t_0)$ has simple zeros for t_0 if

$$|\rho_0 y_3^3 + \mu A + \frac{11}{18}\eta_1| < f_0\sqrt{B_1^2 + B_2^2}. \tag{57}$$

Case B: In the presence of noise, by (45), we have

$$\sigma_r^2 = \frac{1}{2\pi}\int_{-\infty}^{+\infty}\left[\int_{-\infty}^{+\infty} l(t)\cos(\omega t)dt\right]^2 d\omega. \tag{58}$$

When there is noise, we see that $M(t_0)$ has simple zeros for t_0 in the mean-square sense if

$$\left(\rho_0 y_3^3 + \mu A + \frac{11}{18}\eta_1\right)^2 < f_0^2(B_1^2 + B_2^2) + \sigma_r^2. \tag{59}$$

For the numerical verification part, on the basis of introducing noise by Monte Carlo method, we use the Runge–Kutta method to carry out the following numerical simulations to verify the above results and show the complicated dynamics of system (48)–(50). We take $\varepsilon = 0.01$ and $\eta_1 = 0.1$. Using (57), the chaotic thresholds of systems (48)–(50) with $\delta = 0$ and $\rho_0 = 0.5$ for $\mu = 0.05,\ 0.2,\ 0.4,$ and 0.8 are shown in Fig. 3(a), while the chaotic thresholds of (48)–(50) with $\delta = 0$ and $\mu = 0.5$ obtained by (57) for $\rho_0 = 0.1,\ 0.4,\ 0.7,$ and 1 are shown in Fig. 3(b). The thresholds for chaos increase as both ρ_0 and damping coefficient μ increase (see Fig. 3). Namely, in a certain range, for the system under the same periodic excitation amplitude f_0 and frequency Ω, the smaller the value of ρ_0 and damping coefficient μ, the more easily the possible chaos of the system will be induced, making the corresponding system in a chaotic state. The chaotic thresholds of (48)–(50) with $\rho_0 = 0.9$ and $\Omega = 1.8$ from (59) for $\mu = 0.05,\ 0.2,\ 0.4,$ and 0.8 are shown in Fig. 4(a). The chaotic thresholds of (48)–(50) with $\mu = 0.9$ and $f_0 = 1$ from (59) for $\rho_0 = 0.1,\ 0.4,\ 0.7,$ and 1 are shown in Fig. 4(b). Within a certain parameter range, the thresholds for chaos increase as both ρ_0 and damping coefficient μ increase in (δ, f_0) and (Ω, δ) planes, respectively. And for the noise intensity δ within a certain range, the greater the noise intensity, the more easily the possible chaos can be induced. The critical surface of (48)–(50) with $\delta = 0$ and $\rho_0 = 0.5$ in (Ω, μ, f_0) space is shown in Fig. 5(a), and that for $\rho_0 = 0.1,\ \mu = 0.9,$ and $f_0 = 1$ in (Ω, η_1, δ) space is shown in Fig. 5(b). For Figs. 3–5, the area above the boundary will generate complicated dynamics near the unperturbed heteroclinic orbits.

Taking $\varepsilon = 0.01,\ \mu = 0.08,\ \Omega = 1.6,\ \eta_1 = 0.1,\ \rho_0 = 0.9,\ \delta = 0,$ and $f_0 = 1.2$, periodic motion in systems (48)–(50) is shown in Fig. 6(a). To further show the complicated dynamics of

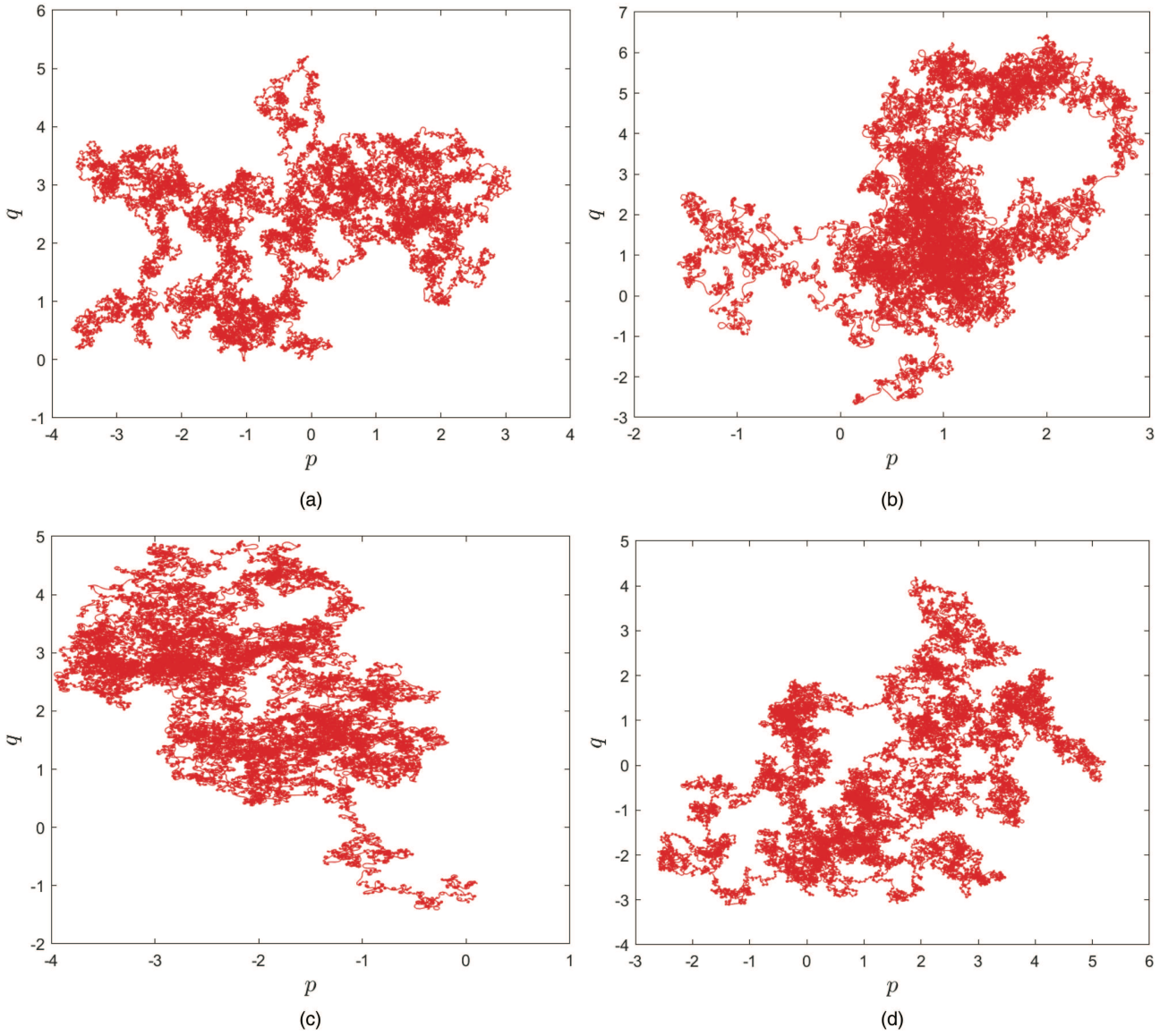

FIG. 10. The phase portraits of systems (48)–(50) with $\varepsilon = 0.01$, $\mu = 0.08$, $\Omega = 1.6$, $\eta_1 = 0.1$, and $\rho_0 = 0.9$ in the new coordinates (p, q) for $f_0 = 8$ and different δ: (a) $\delta = 0.000\,005$, (b) $\delta = 0.1$, (c) $\delta = 2$, and (d) $\delta = 5$.

systems (48)–(50), the following choice of parameters corresponding to numerical simulations ensure the existence of the transverse heteroclinic orbit. In the absence of noise, so that $\delta = 0$, the transient chaotic motion of systems (48)–(50) with $f_0 = 3$ is in Fig. 6(b). After a period of transient chaotic motion near the unperturbed heteroclinic orbits, its solution diverges rapidly. Chaotic motions with $\delta = 0$ and $f_0 = 3.5$, 6.4, 8, and 16 are shown in Figs. 6(c)–6(f). In range, with the increase in periodic excitation amplitude f_0, the chaotic degree of the motion shown by this system in the phase portraits will generally deepen. Among them, Fig. 6(d) shows divergence of trajectories after a chaotic transient. This is related to the structure of the heteroclinic orbits. In the interests of clarity, we also give the phase portraits and time series without noise excitation for $f_0 = 18.5$ in Fig. 7. It can be seen from this figure that the system shows strong complexity at this time, i.e., the degree of chaotic motion at this time is further deepened compared with that when periodic excitation amplitude f_0 takes other values. With noise chaotic motions of system (48)–(50) with $f_0 = 8$ and $\delta = 0.000\,005$, 0.1, 2, and 5 are shown in Figs. 8(a)–8(d). With the increase in δ, the chaotic motion in Fig. 8(a) shows further

dissipation, which deepens the degree for chaos. However, as noise intensity continues to increase, the dissipation phenomenon weakens, and the degree of chaotic motion in this system is also weakened, as shown in Figs. 8(c) and 8(d). These reveal that changing noise intensity can enhance or suppress chaos of this system. For Figs. 6(b) and 8(a), we know in the case of the same periodic excitation intensity $f_0 = 8$, even if the intensity of the noise introduced to the system is very small $\delta = 0.000\,005$, it also has a certain influence on phase portraits, chaotic state, and degree and performances in other aspects of the system.

The method of the 0-1 test[44–46] is utilized to further identify the presence of chaos. In this method, regular behavior corresponds to the test result giving a value that is close to 0, the trajectories in the new coordinates being bounded. Chaotic behavior corresponds to a test result of 1, with unbounded trajectories that are Brownian-like. The regular and chaotic behavior of dynamical systems (48)–(50) will be judged through the correlation coefficient K_c: the system's dynamical behavior is regular when $K_c \approx 0$, and chaotic when $K_c \approx 1$. Then, applying the 0-1 test to (48)–(50) in the absence of noise, ($\delta = 0$), the phase portraits in other coordinates $p(n)$ and $q(n)$ for $f_0 = 1.2$, 3, 3.5, 6.4, 8, and 16 are shown in Figs. 9(a)–9(f), with corresponding values of $K_c = 0.0023$ ($K_c \to 0$) and $K_c = 0.9713$, 0.9882, 0.9912, 0.9930, and 0.9991 ($K_c \to 1$), respectively. The phase portraits in $p(n)$ and $q(n)$ variables for $\delta = 0.000\,005$, 0.1, 2, and 5 are in Figs. 10(a)–10(d), corresponding to $K_c = 0.9947$, 0.9976, 0.9989, and 0.9965 ($K_c \to 1$), respectively. Thus, Figs. 9 and 10 and the value of the associated K_c provide further tests and verify periodic and chaotic motion.

IV. CONCLUSIONS

In this study, we have theoretically developed the classical Melnikov method for heteroclinic orbits in deterministic, continuous systems to a class of hybrid piecewise-smooth systems with impulsive effect and noise excitation. We have assumed the unperturbed system to be piecewise Hamiltonian with a pair of piecewise heteroclinic orbits. The two switching manifolds of the system are $x = \alpha$ and $x = \beta$, so that $\mathbb{R}^2 = S_1 \cup \Sigma_1 \cup S_2 \cup \Sigma_2 \cup S_3$, and three subsystems correspond to each of the three zones S_i, $i = 1, 2$, and 3. The trajectory of the perturbed system transversally jumps across Σ_1 by impulsive effect and crosses Σ_2 by applying the reset map describing the impact rule instantaneously. The corresponding random Melnikov function about the heteroclinic orbits is then obtained by measuring the distance of the perturbed stable and unstable manifolds, the methods used in this derivation is different from that in the corresponding homoclinic case, which is caused by the difference between the symmetry of homoclinic orbits and the asymmetry of heteroclinic orbits. Therefore, the derivation method of the homoclinic case cannot be directly used in our this paper, and the relevant methods need to be improved and extended. We overcome this difficulty caused by asymmetry through using the recursive method and the perturbation principle. And criteria for the onset of chaos with and without noise excitation are established. Significantly, the specific form of the non-smooth random Melnikov process we derive is different from previous results. These extend existing results about the classical Melnikov method.

Then the complicated dynamics of a specific piecewise-smooth system with and without noise excitation under the reset maps, impulsive effect, and non-autonomous periodic and damping perturbations are investigated by this extended Melnikov-type method. Analytical results and the effects of parameter excitation and noise on chaos are verified and analyzed through numerical simulations including time series, phase portraits, and the 0-1 test for chaos. The results verify the theoretical part and demonstrate that changing the periodic excitation coefficient or noise intensity can induce or suppress chaos in such hybrid piecewise-smooth systems. Although we have dealt with the heteroclinic case and the existence of chaos in this paper, some global bifurcations for piecewise linear systems should be further analyzed in future.[47]

ACKNOWLEDGMENTS

This work was supported by the National Natural Science Foundation of China (NNSFC) (Nos. 12172340, 11832002, and 11772306), the Zhejiang Provincial Natural Science Foundation of China (Grant No. LY20A020001), the Fundamental Research Funds for the Central Universities, China University of Geosciences (Wuhan) (Nos. CUGGC05 and CUGDCJJ202216), and the Young Top-notch Talent Cultivation Program of Hubei Province.

AUTHOR DECLARATIONS

Conflict of Interest

The authors have no conflicts to disclose.

Author Contributions

Zhouchao Wei: Writing – original draft (lead). **Yuxi Li:** Validation (equal); Visualization (equal). **Irene Moroz:** Writing – review & editing (equal). **Wei Zhang:** Writing – review & editing (equal).

DATA AVAILABILITY

Data sharing is not applicable to this article as no new data were created or analyzed in this study.

REFERENCES

[1] Y. X. Li, Z. C. Wei, W. Zhang, and M. Yi, "Melnikov-type method for a class of hybrid piecewise-smooth systems with impulsive effect and noise excitation: Homoclinic orbits," Chaos **32**, 073119 (2022).
[2] B. Brogliato, *Nonsmooth Mechanics* (Springer, London, 1999).
[3] M. Wiercigroch and E. Pavlovskaia, *Engineering Applications of Non-Smooth Dynamics* (Springer, Dordrecht, 2012).
[4] M. C. Mackey and L. Glass, "Oscillation and chaos in physiological control systems," Science **197**, 287–289 (1977).
[5] Y. Nesterov, "Excessive gap technique in nonsmooth convex minimization," SIAM J. Optim. **16**, 235–249 (2005).
[6] T. Kobori, M. Takahashi, T. Nasu, N. Niwa, and K. Ogasawara, "Seismic response controlled structure with active variable stiffness system," Earthq. Eng. Struct. Dyn. **22**, 925–941 (1993).
[7] N. Blackbeard, H. Erzgräber, and S. Wieczorek, "Shear-induced bifurcations and chaos in models of three coupled lasers," SIAM J. Appl. Dyn. Syst. **10**, 469–509 (2011).
[8] F. R. Wang, H. Z. Liu, Z. C. Wei, and I. Moroz, "Generalized Hopf bifurcation analysis of a towed caster wheel system," Int. J. Non-Linear Mech. **137**, 103789 (2021).

[9]Z. Faghani, F. Nazarimehr, S. Jafari, and J. C. Sprott, "Simple chaotic systems with specific analytical solutions," Int. J. Bifurc. Chaos **29**, 1950116 (2019).
[10]Z. C. Wei, Y. Y. Li, B. Sang, Y. Liu, and W. Zhang, "Complex dynamical behaviors in a 3D simple chaotic flow with 3D stable or 3D unstable manifolds of a single equilibrium," Int. J. Bifurc. Chaos **29**, 1950095 (2019).
[11]Z. Faghani, F. Nazarimehr, S. Jafari, and J. C. Sprott, "A new category of three-dimensional chaotic flows with identical eigenvalues," Int. J. Bifurc. Chaos **30**, 2050026 (2020).
[12]Z. C. Wei, B. Zhu, J. Yang, M. Perc, and M. Slavinec, "Bifurcation analysis of two disc dynamos with viscous friction and multiple time delays," Appl. Math. Comput. **347**, 265–281 (2019).
[13]V. K. Melnikov, "On the stability of the center for time periodic perturbations," Trans. Moscow Math. Soc. **12**, 1–57 (1963). http://mi.mathnet.ru/eng/mmo/v12/p3.
[14]J. Guckenheimer and P. Holmes, *Nonlinear Oscillations, Dynamical Systems and Bifurcations of Vector Fields* (Sprigner, New York, 1997).
[15]S. Wiggins, *Introduction to Applied Nonlinear Dynamical Systems and Chaos* (Sprigner, New York, 2000).
[16]L. Shi, Y. Zou, and T. Kpper, "Melnikov method and detection of chaos for non-smooth systems," Acta Math. Appl. Sin. Engl. Ser. **29**, 881–896 (2013).
[17]M. Kunze, *Non-Smooth Dynamical Systems* (Springer, Berlin, 2000).
[18]J. Castro and J. Alvarez, "Melnikov-type chaos of planar systems with two discontinuities," Int. J. Bifurc. Chaos **25**, 1550027 (2015).
[19]Z. D. Du and W. N. Zhang, "Melnikov method for homoclinic bifurcations in nonlinear impact oscillators," Comput. Math. Appl. **50**, 445–458 (2005).
[20]F. Battelli and M. Fečkan, "Homoclinic trajectories in discontinuous systems," J. Dyn. Differ. Equat. **20**, 337–376 (2008).
[21]F. Battelli and M. Fečkan, "On the chaotic behaviour of discontinuous systems," J. Dyn. Differ. Equat. **23**, 495–540 (2011).
[22]F. Battelli and M. Fečkan, "Bifurcation and chaos near sliding homoclinics," J. Differ. Equat. **248**, 2227–2262 (2010).
[23]F. Battelli and M. Fečkan, "Nonsmooth homoclinic orbits, Melnikov functions and chaos in discontinuous systems," Physica D **241**, 1962–1975 (2012).
[24]S. B. Li, W. Zhang, and Y. X. Hao, "Melnikov-type method for a class of discontinuous planar systems and applications," Int. J. Bifurc. Chaos **24**, 1450022 (2014).
[25]A. Granados, S. J. Hogan, and T. M. Seara, "The Melnikov method and subharmonic orbits in a piecewise-smooth system," SIAM J. Appl. Dyn. Syst. **11**, 801–830 (2012).
[26]S. B. Li, W. S. Ma, W. Zhang, and Y. X. Hao, "Melnikov method for a class of planar hybrid piecewise-smooth systems," Int. J. Bifurc. Chaos **26**, 1650030 (2016).
[27]S. B. Li, C. Shen, W. Zhang, and Y. X. Hao, "The Melnikov method of heteroclinic orbits for a class of planar hybrid piecewise-smooth systems and application," Nonlinear Dyn. **85**, 1091–1104 (2016).
[28]S. B. Li, H. L. Wu, X. X. Zhou, T. T. Wang, and W. Zhang, "Theoretical and experimental studies of global dynamics for a class of bistable nonlinear impact oscillators with bilateral rigid constraints," Int. J. Non-Linear Mech. **133**, 103720 (2021).
[29]S. B. Li, H. L. Wu, and J. N. Chen, "Global dynamics and performance of vibration reduction for a new vibro-impact bistable nonlinear energy sink," Int. J. Non-Linear Mech. **139**, 103891 (2021).
[30]R. L. Tian, Y. F. Zhou, B. L. Zhang, and X. W. Yang, "Chaotic threshold for a class of impulsive differential system," Nonlinear Dyn. **83**, 2229–2240 (2016).
[31]R. L. Tian, Y. F. Zhou, Y. Z. Wang, W. J. Feng, and X. W. Yang, "Chaotic threshold for non-smooth system with multiple impulse effect," Nonlinear Dyn. **85**, 1849–1863 (2016).
[32]R. L. Tian, T. Wang, Y. F. Zhou, J. Li, and S. T. Zhu, "Heteroclinic chaotic threshold in a nonsmooth system with jump discontinuities," Int. J. Bifurc. Chaos **30**, 2050141 (2020).
[33]S. B. Li, T. T. Wang, and X. L. Bian, "Global dynamics for a class of new bistable nonlinear oscillators with bilateral elastic collisions," Int. J. Dyn. Control **9**, 885–900 (2021).
[34]H. Zheng and Y. H. Xia, "Chaotic threshold of a class of hybrid piecewise-smooth system by an impulsive effect via Melnikov-type function," Discret. Contin. Dyn. Syst. Ser. B **27**, 6353 (2022).
[35]A. R. Bulsara, W. C. Schieve, and E. W. Jacobs, "Homoclinic chaos in systems perturbed by weak Langevin noise," Phys. Rev. A **41**, 668–681 (1990).
[36]M. Frey and E. Simiu, "Noise-induced chaos and phase space flux," Physica D **63**, 321–340 (1993).
[37]H. Lin and S. C. S. Yim, "Analysis of a nonlinear system exhibiting chaotic, noisy chaotic, and random behaviors," J. Appl. Mech. **63**, 509–516 (1996).
[38]Y. M. Lei, F. Zhang, and X. Z. Shao, "Chaos and chaos control of the Frenkel–Kontorova model with dichotomous noise," Int. J. Bifurc. Chaos **27**, 1750052 (2017).
[39]E. L. Chen, W. C. Xing, M. Q. Wang, W. L. Ma, and Y. J. Chang, "Study on chaos of nonlinear suspension system with fractional-order derivative under random excitation," Chaos Solit. Fract. **152**, 111300 (2021).
[40]D. Liu, Y. Xu, and J. Li, "Randomly-disordered-periodic-induced chaos in a piezoelectric vibration energy harvester system with fractional-order physical properties," J. Sound Vibr. **339**, 182–196 (2017).
[41]D. Liu and Y. Xu, "Random disordered periodical input induced chaos in discontinuous systems," Int. J. Bifurc. Chaos **29**, 1950002 (2019).
[42]E. Simiu, "A unified theory of deterministic and noise-induced transitions: Melnikov processes and their application in engineering, physics and neuroscience," AIP Conf. Proc. **502**, 266–271 (2000).
[43]X. L. Yang, Y. Xu, and Z. K. Sun, "Effect of Gaussian white noise on the dynamical behaviors of an extended Duffing-van der Pol oscillator," Int. J. Bifurc. Chaos **16**, 2587–2600 (2006).
[44]G. A. Gottwald and I. Melbourne, "A new test for chaos in deterministic systems," Proc. R. Soc. Lond. Ser. A **460**, 603–611 (2004).
[45]K. H. Sun, X. Liu, and C. X. Zhu, "The 0–1 test algorithm for chaos and its applications," Chin. Phys. B **19**, 110510 (2010).
[46]L. G. Yuan, Q. G. Yang, and C. B. Zeng, "Chaos detection and parameter identification in fractional-order chaotic systems with delay," Nonlinear Dyn. **73**, 439–448 (2013).
[47]Y. M. Lei and F. Zheng, "Stochastic chaos induced by diffusion processes with identical spectral density but different probability density functions," Chaos **26**, 123111 (2016).